CDF/PHYS/CDF/CDFR/10013
version 4

A Search of the Low-Mass Dimuon Data at High p_T

Chris Hays[1] and Ashutosh Kotwal[2]
[1] *University of Oxford,* [2] *Duke University*

July 14, 2010

Recent studies of multilepton production from both astrophysical and collider sources have been unable to explain the data in terms of known processes. New models of gauge groups with a low energy scale coupling to the standard model through a high energy scale could explain these excesses. We perform a general search for new sources of muon pairs at a low energy scale and produced with high p_T at the Tevatron. We find the data to be consistent with the expected background.

Contents

Contents

1 Introduction

A recent CDF study of the low-p_T dimuon data found high multiplicities of muon candidates in a narrow cone, at rates significantly higher than the estimated background [1]. Studies of astrophysical sources, such as INTEGRAL [2] and PAMELA [3], have found excess production of electrons, but not protons. In order to explain the astrophysical excesses, models have been proposed with a U(1) gauge group whose gauge boson is at the GeV scale and couples weakly to the standard model [4, 5]. Such gauge bosons could be produced at the Tevatron, either directly or through radiation from states bound by the new gauge interaction.

Generically, a high-mass particle decaying to low-mass particles that each decay to muon pairs will result in highly boosted dimuons. We perform a general search for low-mass dimuon production at high p_T. To maximize acceptance to new sources of boosted muon pairs, we select events using only the muon and COT detectors, thus allowing for long-lived sources and the associated production of hadrons.

2 Event Selection

Our search strategy is to maximize acceptance while selecting a high-purity sample of dimuons. We use the high-p_T muon trigger to allow tight selection on one of the muon candidates, and to provide an unbiased sample of additional candidates. We use muons fiducial to the CMU and CMP detectors, significantly reducing the rate of punch-through hadrons. The p_T threshold on the unbiased muon is as low as possible while still minimizing inefficiency from range-out.

Our data set consists of 2.2 fb^{-1} collected with the high-p_T CMUP trigger and passing the standard CMUP-plus-silicon good run list. We select events with a trigger CMUP muon and an additional (lower-p_T) muon candidate within a $\Delta R < 0.5$ cone (Table 1), rejecting cosmic-ray events using the COT-based filter [6]. We ensure high trigger efficiency by requiring one muon candidate to have $p_T > 20$ GeV, where p_T is measured using the default track reconstruction. We ensure high efficiency for muon identification by requiring $p_T > 3$ GeV for the other candidate. To reduce potential background from punch-through showers, we reject additional muon candidates with a CMU or CMP stub in the cone.

Both muons are identified based on standard COT and muon-chamber selection (Table 2), with no silicon or calorimeter requirements. We use a variable ("number of transitions") that counts the number of times the COT hit residuals move from one side of the reconstructed track to the other as the hit radius increases. A minimum requirement on this variable has been shown to reduce background from decays in flight in the COT [7].

We separate the dimuon sample into opposite- and same-charge muons, since the backgrounds and potential signals are different for the different samples. Our probe distribution

Requirement
CMUP trigger
Two CMUP muons in $\Delta R < 0.5$ cone
$p_T^{\mu 1} > 20$ GeV, $p_T^{\mu 2} > 3$ GeV
No additional loose muon candidate in cone

Table 1: The event selection for the search.

Variable	Standard requirement	Loose requirement
CMUP-fiducial	Yes	Yes
CMU, CMP stubs	Both stubs required	≥ 1 stub required
Δx(track, CMU stub)	< 30 cm $\cdot$ GeV$/p_T$ ($p_T < 10$ GeV) < 3 cm ($p_T \geq 10$ GeV)	None
Δx(track, CMP stub)	< 75 cm $\cdot$ GeV$/p_T$ ($p_T < 15$ GeV) < 5 cm ($p_T \geq 15$ GeV)	None
# axial COT SL with ≥ 5 hits	≥ 3	≥ 3
# stereo COT SL with ≥ 5 hits	≥ 3	≥ 3
COT χ^2/d.o.f.	≤ 2	≤ 2
# transitions (highest p_T muon)	≥ 35	N/A

Table 2: The identification requirements applied to muons in the event selection. The loose muon definition is used to reject additional muon candidates in the cone.

is the dimuon mass distribution, since a wide class of new physics processes would appear as a narrow peak in this distribution. Figure 1 shows the mass and log-mass distributions in the data without the ΔR cut and loose muon rejection.

3 Background Estimation

The dominant backgrounds to low-mass muon pairs at high p_T are: sequential B hadron decays to muon pairs; light-hadron resonance decays to muon pairs; overlap of a π or K with a heavy-flavor or gauge-boson decay, where the π or K decays to a muon, sails through the calorimeter to the muon chambers, or produces a hadronic shower that results in track stubs in the muon chambers (punch-through); and Drell-Yan production. We have investigated potential background from photon conversions and $t\bar{t}$ and WW production, and found them to be negligible.

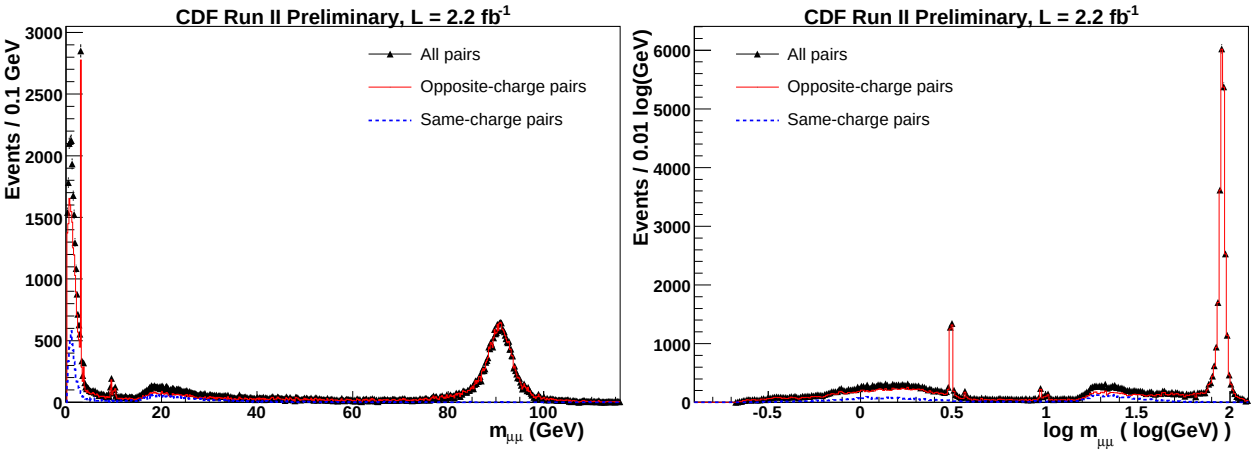

Figure 1: The opposite-charge (solid red), same-charge (dashed blue), and combined (triangles) mass (left) and log-mass (right) distributions of a trigger muon and a second muon candidate passing all event selection except the ΔR cut and loose muon rejection.

3.1 Hadrons Decaying to Muon Pairs

The sources of hadrons decaying to muon pairs are predominantly J/ψ production and sequential semileptonic B decay (Table 3). The production of B hadrons at the Tevatron can be modelled using inclusive jet production in PYTHIA, which includes b-quarks produced from gluon splitting. Since the production rates have sizable uncertainties, we normalize to $B \to J/\psi K$ decays in the data collected with the high-p_T CMUP trigger. Thus, we mainly rely on PYTHIA and EVTGEN to provide the kinematic and decay angular distributions of the B hadrons, and their relative branching ratios. To reduce this dependence on Monte Carlo, we have applied correction factors to match various production and decay parameters to CDF measurements (Sec. 4).

The PYTHIA inclusive jet sample is generated with version 6.325 and a $p_T > 15$ GeV threshold in the production. We use the standard underlying event parameters from Rick Field ("tune A") and apply a HEPG requirement of a muon with $p_T > 17$ GeV and $|\eta| < 1.2$ on the generated events. A good run list obtained via the B-group procedure is used to generate 250 billion events, of which 4.5 million pass the filter.

We select $B \to J/\psi K$ events by matching a track with $p_T > 2$ GeV to a reconstructed J/ψ candidate. The J/ψ candidate is defined as an opposite-charge muon pair passing our event selection and having reconstructed mass in the range $3 - 3.15$ GeV. The mass of the two muons and the additional K candidate fit using CTVMFT is shown in Fig. 2. To maximize the statistical sensitivity, we normalize the MC to the data using the mass difference between the $K\mu\mu$ and $\mu\mu$ combinations (Fig. 2). This difference removes the resolution contribution to the muon pair. The normalization region is taken to be $2.14 - 2.22$ GeV and the combinatoric background is estimated using the two sideband mass regions of

Source	Fraction
$J/\psi \to \mu\mu$	43.9%
$B_d \to D^{\pm}\mu\nu \to \mu\mu X$	20.5%
$B^{\pm} \to D\mu\nu \to \mu\mu X$	14.4%
Coincident B and/or D decays	6.6%
$B_s \to D_s^{\pm}\mu\nu \to \mu\mu X$	5.2%
$\eta \to \mu\mu\gamma$	1.7%
$\rho \to \mu\mu$	1.6%
$\phi \to \mu\mu$	1.5%
$B^{\pm}B^{\mp} \to \mu\mu X$	0.9%
$\Lambda_b \to \mu\mu X$	0.9%
$B_d\bar{B}_d \to \mu\mu X$	0.8%
$\psi' \to \mu\mu$	0.6%
$D\bar{D} \to \mu\mu X$	0.5%
$D^{\pm}D^{\mp} \to \mu\mu X$	0.3%

Table 3: The relative generator-level sources of dimuons ($p_T^{\mu 1} > 20$ GeV, $p_T^{\mu 2} > 3$ GeV) from PYTHIA inclusive jet production. A number of other modes contribute at the $< 0.1\%$ level. The corrections described in Section 4 have not been applied.

$2.04 - 2.12$ GeV and $2.24 - 2.32$ GeV.

The rate of J/ψ production is generally not well modelled. We include color octet production in our PYTHIA sample using the default parameters. This significantly overestimates the direct production fraction, so we reweight J/ψ candidates without a B-hadron parent at the generator level such that the prompt production fraction is consistent with the CDF measurement performed with 39.7 pb^{-1} in the beginning of Run II [8]. The measured fraction of prompt J/ψ production is measured up to a $p_T^{J/\psi}$ of 20 GeV. Because of our generator-level filter, we normalize in the region just above the measurement, $20 < p_T^{J/\psi} < 23$ GeV. Using the measurements in the highest p_T bins, we extrapolate the measured prompt fraction to $48 \pm 10\%$ in this range (Table 4). In addition, to obtain the correct rate of J/ψ mesons from B hadron decays, we apply a weight to match the PDG branching ratio of $B \to J/\psi X$ (Sec. 4).

A potential source of uncertainty in our normalization procedure is the efficiency for finding a $B \to J/\psi K$ candidate compared to the efficiency for finding muon pairs from other hadron decays. Since the track-finding efficiency is modelled to better than 1% accuracy for tracks with $p_T > 2$ GeV [9], the uncertainty on finding the kaon track is negligible. The muon identification for the low-p_T muon could cause a bias if the ratio of data to MC efficiencies has a momentum dependence, and there is a difference between the p_T distributions of muons from $B \to J/\psi K$ decays and from other sources.

We study the efficiency for muons to pass our standard requirements, relative to the

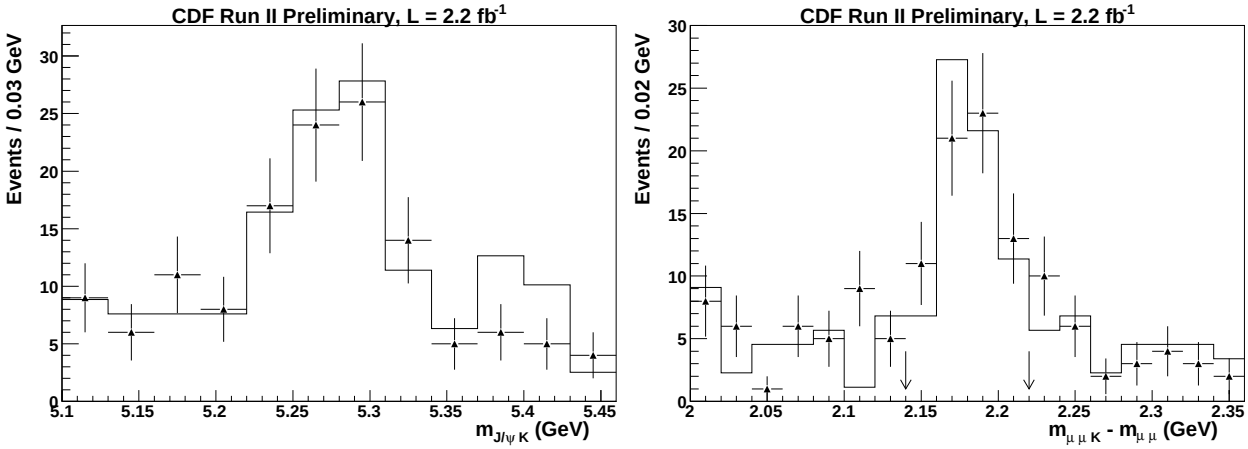

Figure 2: Left: The mass distribution of a $K^{\pm}$ and two opposite-charge muons passing the event selection and $3 < m_{\mu\mu} < 3.15$ GeV. Right: The mass difference of the $K^{\pm}\mu\mu$ and $\mu\mu$ combinations. The PYTHIA inclusive jet sample (histogram) is normalized to the data (triangles) after subtracting combinatoric background using the sidebands.

p_T Range	Direct J/ψ Fraction
12-14 GeV	$66.3 \pm 2.1\%$
14-17 GeV	$61.3 \pm 2.7\%$
17-20 GeV	$53.6 \pm 4.8\%$
20-23 GeV	$48 \pm 10\%$

Table 4: The direct J/ψ fraction as measured by CDF [8] in the J/ψ p_T range of 12-20 GeV, and our extrapolation to the p_T range 20-23 GeV.

loose requirements, using J/ψ decays. Starting with a pair of opposite-charge muons with $3 < m_{\mu\mu} < 3.15$ GeV, where one high-p_T muon passes the standard selection and the second muon passes the loose selection, we calculate the rate for the second muon to pass the standard selection as a function of p_T (Fig. 3). We correct for background using same-charge pairs, assuming equal rates of same-charge and opposite-charge muon candidates in the background. The ratio of data to MC efficiencies shows no significant momentum dependence.

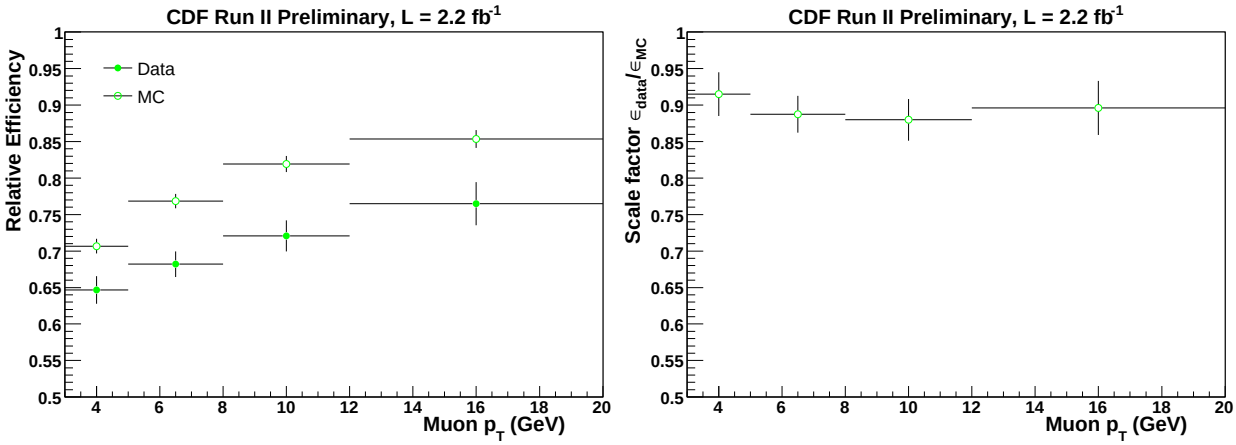

Figure 3: Left: The efficiency for a muon to pass the standard identification, relative to the loose identification. The efficiency is shown as a function of p_T for data (closed circles) and MC (open circles). Right: The ratio of data to MC efficiencies, as a function of p_T. There is no significant momentum dependence.

3.2 Pion and Kaon Background

Pions and kaons contribute to the background primarily when their showers are late in the calorimeter, thus leaking into the muon chambers ("punch-through"). A single shower can produce multiple muon stubs ("correlated fakes"), resulting in the selected dimuon final state. A separate (smaller) source of background comes from the decay of a low-momentum pion or kaon in flight, typically produced in association with a muon from a semileptonic B- or D-hadron decay.

The sources of pion and kaon background can be separated into the following components:

1. Trigger muon plus low-p_T punch-through or decay in flight
2. Low-p_T muon plus trigger punch-through
3. Trigger punch-through plus low-p_T punch-through or decay in flight

4. Trigger punch-through producing two stubs plus low-p_T track

5. Low-p_T punch-through producing two stubs plus high-p_T track,

where the first three are uncorrelated and the last two are correlated. In the correlated background, one of the two stubs produced by the punch-through is attached to the additional track.

We model the correlated and low-p_T muon components (backgrounds 2, 4, and 5) using a sample with a low-p_T muon candidate and a trigger candidate that fails the CMU or CMP Δx requirement. A pass/fail ratio for punch-through is applied to this sample to obtain a background prediction. The remaining components (backgrounds 1 and 3) are modelled by selecting a trigger candidate and applying a fake rate to surrounding low-p_T tracks. To prevent double-counting of background 3 (two uncorrelated fake muons), we explicitly remove the expected low-p_T fake contribution from the sample of a low-p_T candidate plus trigger candidate failing the Δx cuts.

3.2.1 High-p_T π/K Trigger Candidate Background

Backgrounds from a low-p_T muon candidate plus punch-through and correlated punch-through (2, 4, and 5 above) passing the trigger requirements are estimated by applying a pass/fail ratio to a sample of low-p_T muons plus trigger candidates failing either the CMU or CMP Δx cuts (but passing the trigger requirements of CMU $|\Delta x| < 10$ cm and CMP $|\Delta x| < 20$ cm). We expect the pass/fail ratio to accurately model punch-through producing either one or two stubs (i.e., both uncorrelated and correlated background). We test this assumption by studying the CMU and CMP Δx distributions in samples with a single trigger candidate and with a trigger candidate and an additional same-sign muon candidate. We find good agreement in the Δx distributions between the two samples.

To account for possible differences in pass/fail ratio for pion and kaons, we separately measure the ratio for pions (in $K_s \to \pi\pi$ decays) and kaons (in $D \to K\pi$ decays). The kaon and pion fake ratios are found to be equivalent within the statistical uncertainties, indicating dominance of punch-through over decays in flight, and are thus combined into a single fake ratio to be applied to all trigger candidates failing the Δx requirement. We define the uncertainty on this fake ratio to be that of the difference between pion and kaon fake ratios, covering all possible variations of the $\pi : K$ ratio in the sample to which it is applied.

High-p_T Kaon Fake Ratio

To reconstruct a $D \to K\pi$ peak, we select a trigger muon candidate with no surrounding loose muon and perform a CTVMFT fit with all opposite-charge COT-fiducial tracks with $p_T > 2$ GeV and $|\cot\theta| < 1.2$. We require the fit χ^2 to be less than 20, $L_{2D} > 1$ mm, and $L_{2D}/\sigma(L_{2D}) > 5$. The resulting distributions, shown in Fig. 4, are fit to a first-order polynomial background plus a gaussian signal in the D^0 mass region. The polynomial background is integrated from $1.84 - 1.89$ GeV and subtracted from the observed number of events in

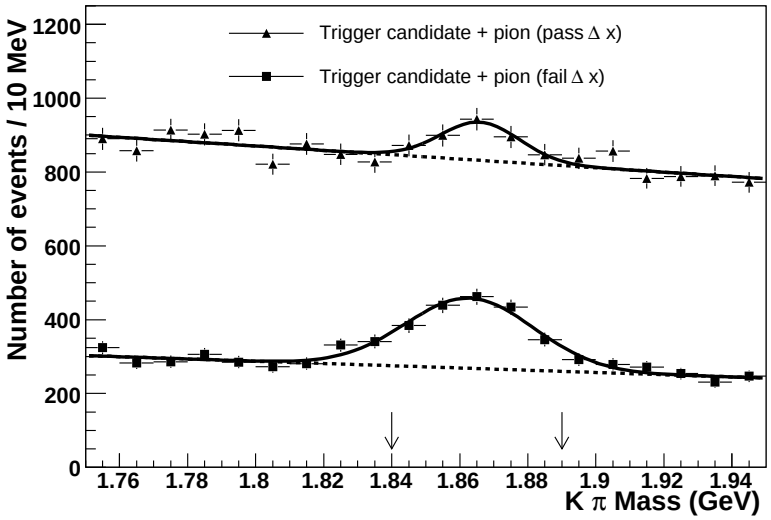

Figure 4: The mass distribution of a $p_T > 2$ GeV track paired with a trigger candidate passing (triangles) or failing (squares) the Δx cuts. The distribution is obtained from a CTVMFT fit with the trigger candidate given the kaon mass and the track given the pion mass. The distributions are fit to a first-order polynomial plus a gaussian.

this range. We obtain 296 ± 68 (727 ± 49) D^0 decays with the trigger candidate passing (failing) the Δx cuts. From these numbers we obtain a kaon fake ratio of 0.41 ± 0.10.

High-p_T Pion Fake Ratio

We reconstruct a $K_s \to \pi\pi$ peak using a trigger muon candidate with no surrounding loose muon and an opposite-charge COT-fiducial track with $p_T > 2$ GeV, $|\cot\theta| < 1.2$, at least 3 (3) axial (stereo) superlayers with at least 5 hits, and COT $\chi^2/\text{dof} < 2$. We require the CTVMFT fit χ^2 to be less than 15, $L_{2D} > 3$ cm, and $L_{2D}/\sigma(L_{2D}) > 5$. The resulting mass distributions for trigger muons passing and failing the Δx requirements are shown in Fig. 5.

The background shapes for events passing (failing) the Δx cuts are obtained from inclusive jet MC generated as described in Sec. 3.1 with a filter on a muon (pion) with $p_T > 17$ GeV. The MC is normalized using an average of the sideband regions 370-450 MeV and 570-650 MeV. Events are selected in the pion-filtered sample using the data selection without the muon stub requirement, and removing events with a generated K_s within $\Delta\phi = 0.05$ of a candidate track.

Taking the difference between data and normalized MC in the mass range 470-550 MeV gives 1040 ± 113 candidates passing the Δx cuts and 1808 ± 92 candidates failing the Δx

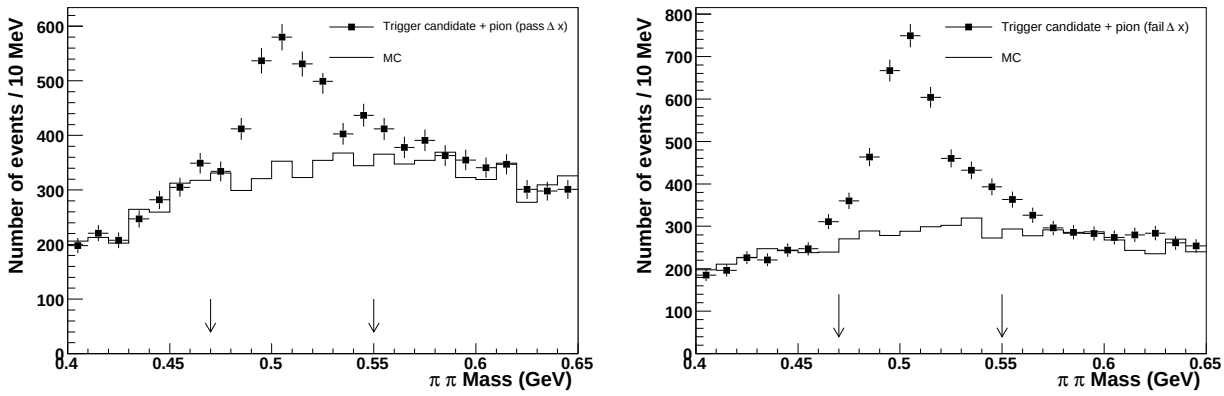

Figure 5: The mass distribution of a $p_T > 2$ GeV track paired with a trigger candidate passing (left) or failing (right) the Δx cuts. The distribution is obtained from a CTVMFT fit with the tracks given the pion mass.

cuts. From these numbers we obtain a pass-to-fail ratio of 0.58 ± 0.07 for pions.

High-p_T Average Fake Ratio

Since the fake ratios for pions and kaons are statistically consistent at the 1.4σ level, we combine them into a single ratio to be applied to trigger candidates failing the Δx requirements in the sample with a surrounding low-p_T muon. A weighted average of the results gives 0.52 ± 0.06.

To account for the possibility that the pion and kaon fake ratios are different, we take the uncertainty on the difference between the ratios as the uncertainty on the average. This uncertainty on the difference is our current statistical sensitivity to differences in the two fake ratios, and is 0.12. Thus, the fake ratio to be applied to the high-p_T trigger muon candidate is 0.52 ± 0.12.

To apply the fake ratio, we select a sample passing all the event selection except requiring the trigger muon candidate to fail the Δx cuts (Fig. 6). We subtract the contributions from heavy-flavor and Drell-Yan using PYTHIA samples, and from low-p_T pion and kaons using the track-based fake rate. The residual component includes both uncorrelated sources of fake muons and the correlated source of punch-through producing two muon candidates.

High-p_T Inclusive Fake Ratio

As a cross-check to our fake ratio derived from kaons and pions, we calculate the fake ratio using the inclusive trigger sample. We expect this sample to be composed primarily of pions, after removing contributions of muons from heavy-flavor and gauge-boson decays.

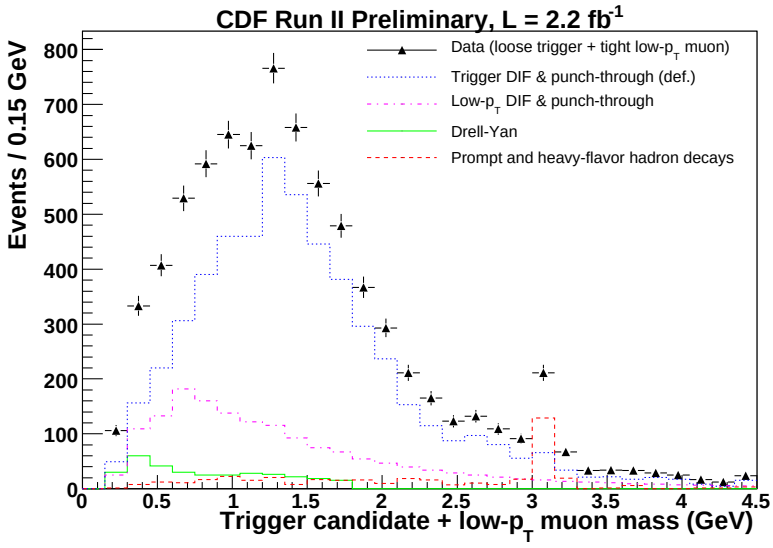

Figure 6: The mass distribution of events with the standard signal selection, except failing the Δx cuts on the trigger muon. After subtracting heavy-flavor (dashed red), Drell-Yan (green), and low-p_T pions and kaons (dash-dotted purple) from the data (triangles), we obtain the contribution from pions and kaons passing the trigger muon requirements (blue dashed). We apply a fake rate to this component to estimate its contribution to the final sample, which include Δx cuts on the trigger muon.

The inclusive fake ratio is calculated in a sample of trigger candidates with no additional loose muon in a $\Delta R < 0.5$ cone (to match the selection requirement) and no additional track with $p_T > 20$ GeV (to suppress Z boson production). To further reduce the contribution from W and Z boson decays we restrict ourselves to the 20-25 GeV p_T region for the fake-ratio measurement.

Heavy-flavor sources of muons are subtracted using the high-p_T PYTHIA sample, normalized using $B \to J/\psi K$ events (Sec. 3.1) with the low-p_T muon selected using loose requirements (Table 2). Muons from W boson decays are not negligible and are subtracted using the standard Electroweak PYTHIA sample, `wewk9m`, normalized in the 35-40 GeV p_T range (Fig. 7). A small Drell-Yan contribution is removed using the normalized PYTHIA sample described in Sec. 3.3. Table 5 shows the numbers of muon candidates in data and predicted by PYTHIA. We use these numbers to derive the following inclusive trigger muon fake ratio:

$$f_t = 0.62 \pm 0.18 \text{ (stat)} \pm 0.06 \text{ (sys)}, \quad (1)$$

where the first uncertainty arises primarily from the $B \to J/\psi K$ statistics used to normalize the PYTHIA MC and the second uncertainty arises from the reweighting of the B-hadron p_T spectrum (Sec. 4.1). This fake ratio is consistent with that obtained from $D \to K\pi$ and

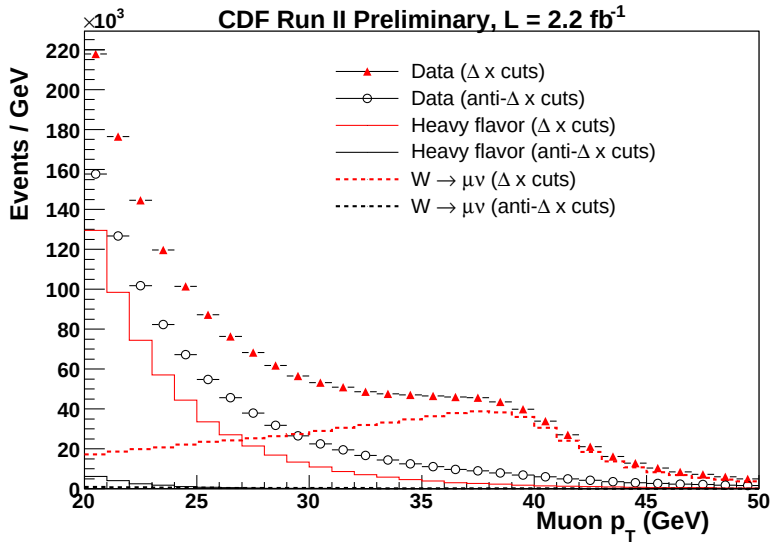

Figure 7: The p_T distribution of trigger muon candidates passing (triangles) and failing (circles) stub-track Δx requirements, in a sample with no additional track with $p_T > 20$ GeV. The histograms show the contribution from heavy flavor (solid) and W boson production (dashed), as predicted by PYTHIA, passing (red) and failing (black) the Δx requirements.

All numbers $\times 10^5$					
Requirements	Data	Heavy-flavor	W bosons	Drell-Yan	Residual
Standard	7.60	3.23 ± 0.93	1.00	0.20	3.17 ± 0.93
Fail Δx	5.35	0.12 ± 0.04	0.04	0.01	5.18 ± 0.04

Table 5: The numbers of trigger muon candidates passing and failing Δx cuts, along with the PYTHIA heavy-flavor and Drell-Yan prediction. The candidates from residual sources are assumed to result from pion and kaon decays in flight and punch-through.

$K \to \pi\pi$ decays (0.52 ± 0.12).

3.2.2 Background from Low-p_T π/K

We use a data-based fake rate to estimate the background from a low-p_T pion or kaon reconstructed as a muon near the trigger muon. The fake rate is the ratio of reconstructed muon candidates to tracks measured in minimum bias data, after subtracting the contribution from muons. The low-p_T π/K background is estimated by multiplying the number of tracks near a trigger muon by the measured fake rate. As a cross-check, we calculate the

Requirements	Data Candidates	PYTHIA Prediction	Residual Sources
Track	2.24×10^6	5245 ± 1054	2.24×10^6
Muon	5945	3756 ± 756	2189 ± 760

Table 6: The numbers of muon and track candidates in minimum bias data, and the PYTHIA predictions. The difference between data and the prediction is presumed to be the contribution from pion and kaon decays in flight and punch-through. The uncertainties shown are the statistical uncertainties on the J/ψ normalization; when applying the fake rate we also include a systematic uncertainty due to the relative D to J/ψ normalization.

fake rate using pions from $K \to \pi\pi$ decays.

To account for the potential larger fraction of kaons in our signal sample (relative to the pion-dominated minimum bias sample), we apply a correction for the relative fake rates of kaons to pions (separated by charge). We take an uncertainty on the correction that covers the possibility that the signal sample is composed entirely of kaon fakes or of pion fakes.

Low-p_T Inclusive Fake Rate

The candidate tracks for the fake rate measurement have the same track requirements as for the low-p_T muon candidates (Table 2). The tracks are selected in a fiducial region overlapping the CMU and CMP chambers, $|\cot\theta| < 0.7$. The numbers of tracks and reconstructed muons in minimum bias data are shown in Table 6.

We subtract heavy-flavor and Drell-Yan sources of muons from the data using a sample of PYTHIA events. The sample is generated with the standard tunes for the Drell-Yan p_T and the underlying event. After event generation, a HEPG filter requires a muon with $p_T > 2.5$ GeV within $|\eta| < 1$. Out of 10 billion generated events, 0.3 million pass the filter. The sources of identified muons are listed in Table 7.

The PYTHIA sample is normalized to data using J/ψ events. To obtain sufficient statistics, we loosen our muon identification to include any muon with a CMU, CMP, or CMX stub, and we require one muon with $p_T > 3$ GeV and a second with $p_T > 2$ GeV. We measure the product of the efficiency times acceptance for these requirements using a high-p_T trigger muon and a second track with $|\cot\theta| < 1.2$. Figure 8 shows the data and MC muon-track mass in the vicinity of the J/ψ peak, before and after the stub requirement. From the gaussian fit we determine the fiducial acceptance times efficiency to be 86.4% (91.2%) and 91.8% (94.7%) for $p_T > 2(3)$ GeV in data and MC, respectively. We apply scale factors of 0.941 and 0.963 for the two muons in the MC to correct for the difference.

As with the high-p_T inclusive jet PYTHIA sample (Sec. 3.1), we reweight the directly produced J/ψ events to match the CDF measurement of the prompt fraction [8], and the $B \to J/\psi X$ events to match the PDG branching ratio (Sec. 4.2). Figure 9 shows the CDF measurement and the reweighted events as a function of J/ψ p_T. A single reweighting factor

Source	Fraction	Source	Fraction
D^0	24.8%	τ	1.2%
$B^\pm$	18.7%	ρ	0.7%
$D^\pm$	18.5%	η	0.7%
B^0	17.2%	ϕ	0.7%
$D_s^\pm$	5.2%	Z/γ^*	0.2%
B_s	4.7%	Ξ_c^0	0.2%
J/ψ	3.1%	$\Xi_c^\pm$	0.2%
Λ_b	2.4%	$\Xi_b^\pm$	0.1%
Λ_c	1.2%	Ξ_b^0	0.1%

Table 7: The relative sources of reconstructed muons with $p_T^\mu > 3$ GeV in low-p_T PYTHIA inclusive QCD and Drell-Yan production, before the reweighting described in Sec. 4.1. A number of other modes contribute at the $< 0.1\%$ level.

for prompt J/ψ production gives good agreement over a range of p_T. Figure 10 shows the $m_{\mu\mu}$ spectrum for data and MC in the vicinity of the J/ψ peak. The background distribution is assumed to be flat in this region, and is estimated using two 150 MeV sidebands neighboring the peak region of $3 - 3.15$ GeV.

The reweighting of J/ψ events fixes the relative production of B hadrons to J/ψ mesons using a CDF measurement. Table 7 shows that the other significant source of muons in the minimum bias data is D-hadron decays. We fix the relative production of D hadrons to J/ψ mesons using the individual CDF measurements [8, 15], as described in Sec. 4.1. Since we normalize the overall sample using J/ψ mesons, all significant sources of muons are effectively constrained by CDF data.

Table 6 shows the data and PYTHIA subtraction, resulting in the following low-p_T fake rate:

$$f_l = 0.098 \pm 0.034\ (\text{stat}) \pm 0.010\ (\text{sys})\%, \tag{2}$$

where the statistical uncertainty arises from the data J/ψ statistics and the systematic uncertainty is due to the relative normalization of D mesons.

Low-p_T Pion Fake Rate

Since the fake rate determined from inclusive minimum bias data contains a subtraction of heavy-flavor muons based on low-p_T PYTHIA Monte Carlo, it is useful to cross-check the measured fake rate with hadrons from a resonant peak. We perform such a cross-check using $K_s \to \pi\pi$ decays.

Kaon decays are selected by requiring one track with $p_T > 3$ GeV and $|\cot\theta| < 0.7$ (the candidate track) and a second track with opposite charge, $p_T > 2$ GeV and either $p_T < 3$ GeV or $|\cot\theta| > 0.7$. The track pair is fit with CTVMFT and required to have $L_{2D} > 3$ cm

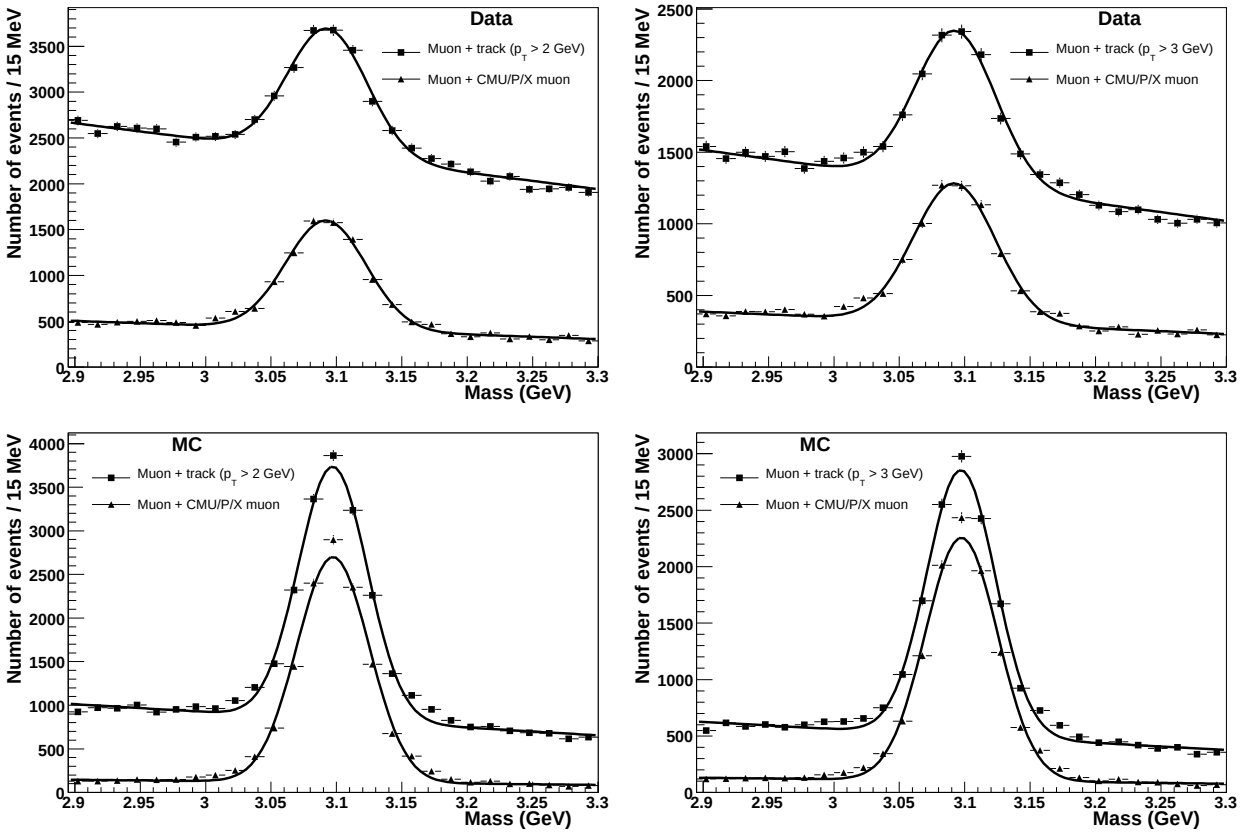

Figure 8: The mass distributions of opposite-charge high-p_T trigger and track candidates (squares) with $p_T > 2$ GeV (left) and 3 GeV (right) in the data (top) and MC (bottom). Also shown are the distributions when the track candidate has a CMU/P/X stub (triangles).

and fit $\chi^2 < 20$. The invariant mass of these pairs is shown in Fig. 11 for all tracks and for tracks passing the muon selection.

To obtain the corresponding fake rate, we estimate the number of $K \to \pi\pi$ events in the peak using the mass range 480-520 MeV. We estimate the background by adding the sideband regions 380-440 MeV and 560-620 MeV, and dividing by 3. The resulting fake rate is $0.11 \pm 0.07\%$, consistent with the fake rate obtained from the inclusive minimum bias sample.

Low-p_T Average Fake Rate

Since we expect the fake candidates in the minimum bias sample to be due primarily to pions, and previous measurements [11] have shown that kaon fake rates are larger than pion fake rates at low momentum, we apply a correction factor to the measured fake rate. The correction factor and corresponding uncertainty cover the scenarios where the fakes in the

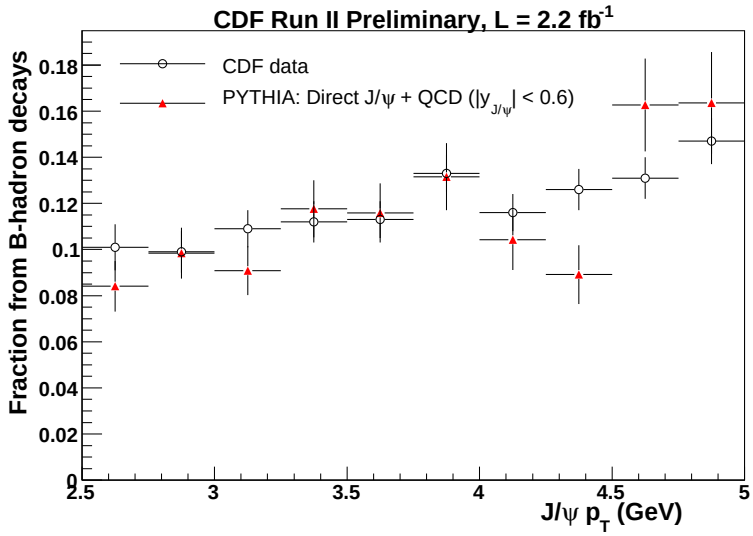

Figure 9: The fraction of J/ψ mesons produced via a B hadron decay, as measured in [8] (open circles), and in this analysis after applying a global correction to prompt J/ψ production in the PYTHIA sample (red triangles).

signal sample are either all pions or all kaons, or some combination in between.

To verify that the prior measurements using decays of D^* mesons are applicable to our sample, we remove the Δx requirement on the low-p_T muon to give a consistent set of cuts. Our resulting fake rate of $0.22 \pm 0.03\%$ is consistent with the prior measurement, assuming the minimum bias sample is composed predominantly of pions. The full set of measured fake rates from the prior analysis is:

- $f_{\pi^+} = 0.24 \pm 0.02\%$,
- $f_{\pi^-} = 0.18 \pm 0.02\%$,
- $f_{K^+} = 0.61 \pm 0.03\%$,
- $f_{K^-} = 0.40 \pm 0.03\%$.

To correct our pion-dominated fake rate, we apply the following ratios to our measured fake rate:

$$(f_{K^+} + f_{\pi^+})/(f_{\pi^+} + f_{\pi^-}) = 2 \pm 1, \quad (3)$$

$$(f_{K^-} + f_{\pi^-})/(f_{\pi^+} + f_{\pi^-}) = 1.4 \pm 0.4, \quad (4)$$

where the uncertainty covers the cases of pure pion and pure kaon fakes in our signal sample. The final fake rates used in our measurement are therefore

$$f_{l^+} = 0.20 \pm 0.10\%, \quad (5)$$

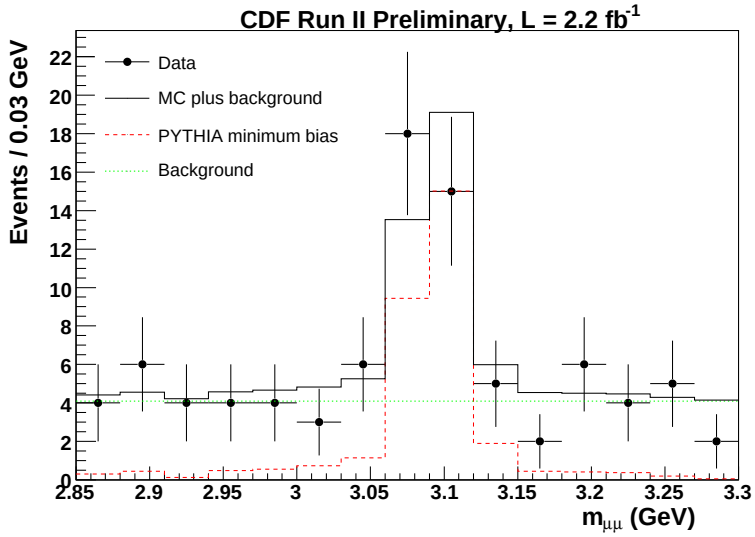

Figure 10: The mass distribution in minimum bias data of a pair of muons with $p_T^{\mu 1} > 3$ GeV and $p_T^{\mu 2} > 2$ GeV and a CMU, CMP, or CMX stub. Also shown are the PYTHIA minimum bias MC sample, the assumed background, and the combined MC plus background. The $3 - 3.15$ GeV mass region is used to normalize the MC, after correcting for background.

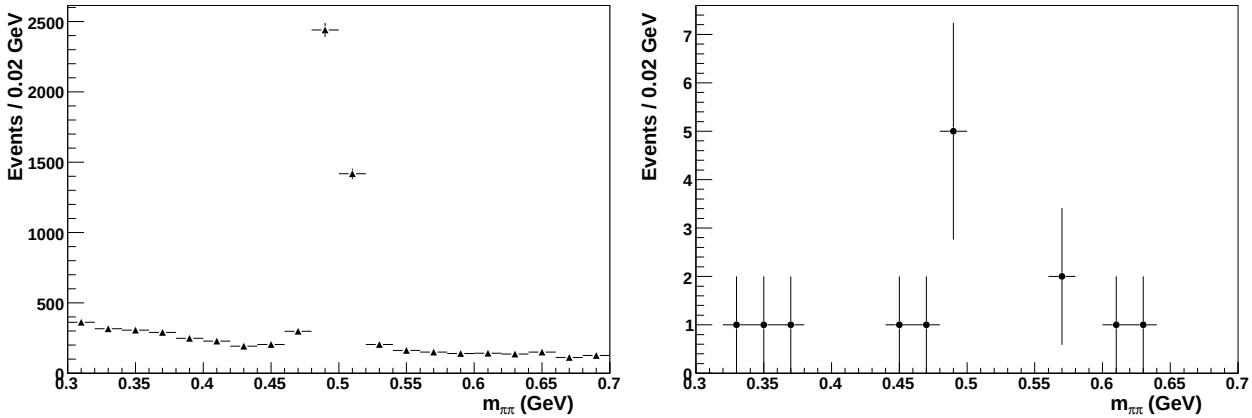

Figure 11: The mass distribution of a $p_T > 3$ GeV candidate track paired with a second track with $p_T > 2$ GeV and either $p_T < 3$ GeV or $|\cot\theta| > 0.7$. The left distribution shows all track pairings, the right shows those where the candidate track passes the muon identification requirements.

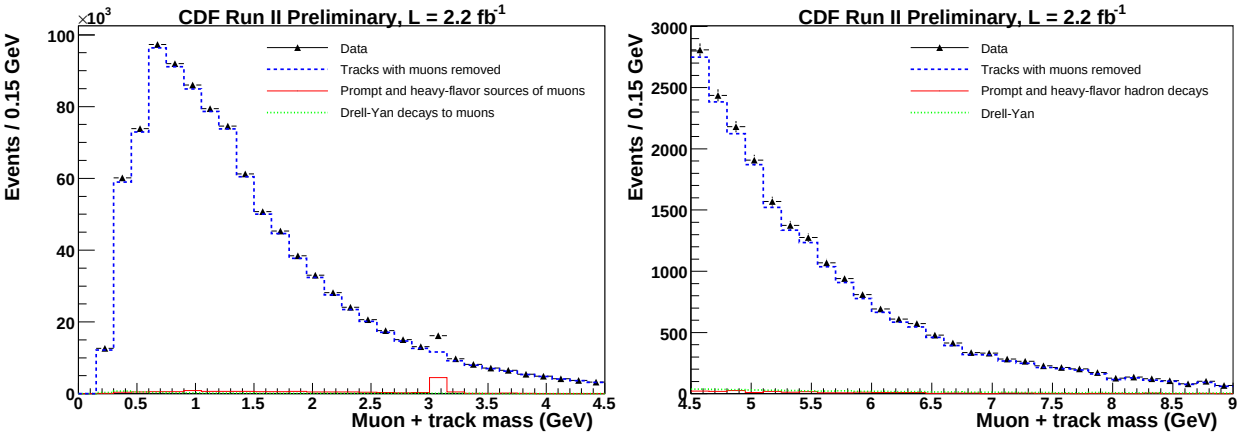

Figure 12: Left: The mass distribution of opposite-charge trigger muon and track combinations, up to 4.5 GeV. Right: The same distribution in the 4.5 - 9 GeV range. The dashed line shows the distribution after subtracting muons from PYTHIA production of hadrons and Drell-Yan.

$$f_{l^-} \quad = \quad 0.14 \pm 0.05\%. \tag{6}$$

These fake rates are applied to $p_T > 3$ GeV tracks in a $\Delta R = 0.5$ cone around a high-p_T trigger muon, after subtracting muons from heavy-flavor decays and Drell-Yan. The mass distribution of this trigger-muon-plus-track sample is shown in Figs. 12 and 13 for opposite- and same-charge muon candidates, respectively.

3.2.3 Correlated π/K Background

By construction, correlated π/K background is included in the sample containing a low-p_T muon candidate and a trigger candidate failing the Δx cuts. The modelling of correlated fake background relies on the applicability of the measured pass/fail ratio to the correlated component of this sample.

We expect the correlated background to be dominated by a high-p_T π/K that punches through and produces two muon stubs, one of which becomes the trigger candidate and the other the nearby low-p_T muon candidate. There are several possible scenarios for the x positions of the two stubs. If the two stubs tend to be near each other, then the single-stub pass/fail ratio is applicable to the two-stub sample. If the two stubs follow the same distribution as the single-stub punch-through and there is no preference in attaching the two stubs to the trigger candidate, then the pass/fail ratio would still be applicable. However, the reconstruction attaches stubs in decreasing order of p_T, so we expect it to preferentially attach the closest stub to the high-p_T trigger candidate. In this scenario, the two-stub sample would have an excess of punch-through relative to our prediction.

To test the applicability of the pass/fail ratio to the two-stub sample, we compare the

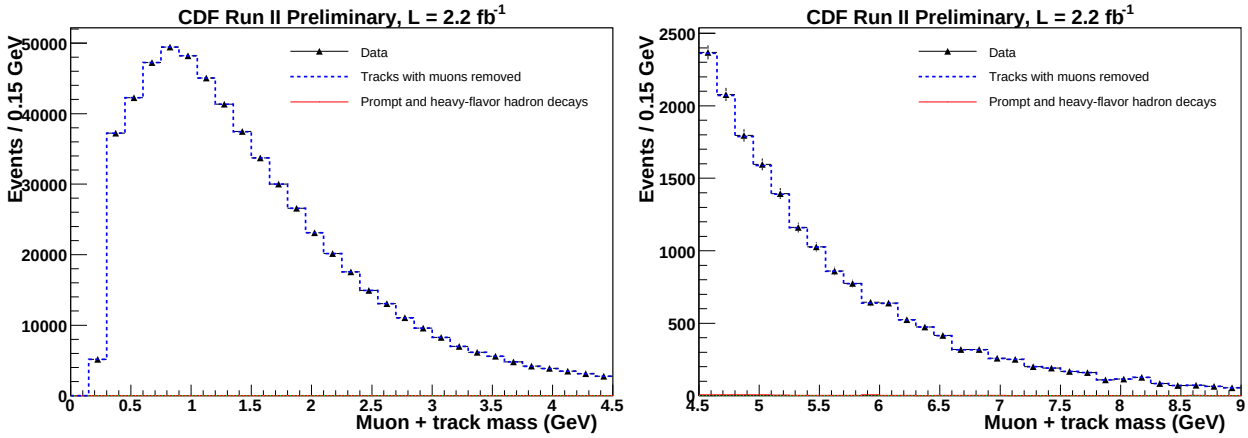

Figure 13: Left: The mass distribution of same-charge trigger muon and track combinations, up to 4.5 GeV. Right: The same distribution in the 4.5 - 9 GeV range. The dashed line shows the distribution after subtracting muons from PYTHIA production of hadrons. Multiplying this distribution by the fake rate gives the predicted background due to a same-charge trigger muon and low-p_T kaon or pion.

Δx distributions for the inclusive trigger sample to the same-charge muon sample, after subtracting the expected contribution from muons passing the trigger. The distributions are in reasonable agreement for both CMU and CMP, as shown in Fig. 14. The Figure shows the inclusive trigger sample scaled to the same-charge sample, as well as the trigger sample with -1σ of the expected muon subtraction. We conclude that the pass/fail ratio is applicable to the two-stub sample within our quoted uncertainty.

3.2.4 First-Principle Estimates

Some insight can be obtained by making rough estimates of fake rates using first-principle physics. Contributions from decays in flight, sail-through, and punch-through can be calculated with relatively few assumptions. We estimate the relative numbers of 3 GeV and 20 GeV muons from kaon and pions with the same momentum (Table 8).

A decay in flight before the COT results in a muon with similar efficiencies to prompt muons. Assuming that the measured momentum is that of the final muon, one needs an original pion or kaon with about twice the momentum of the muon. Using the respective π and K lifetimes (7.8 m and 3.6 m), branching ratios to muons (1 and 0.64), and masses (140 MeV and 490 MeV), and the relativistic factor $\gamma = E/m$, we can calculate the fraction of pions and kaons that decay in the first 50 cm. For 6 GeV π and K, the fractions are 0.15% and 0.70%, respectively. In minimum bias data there are 30 times as many 3 GeV tracks as 6 GeV tracks, reducing the respective fractions to 0.005% and 0.024% at 3 GeV. Finally, there is about a 3:1 ratio of π to K in minimum bias data, so the relative fraction of 3 GeV muons from decays in flight is expected to be 0.01%. A similar calculation for 20

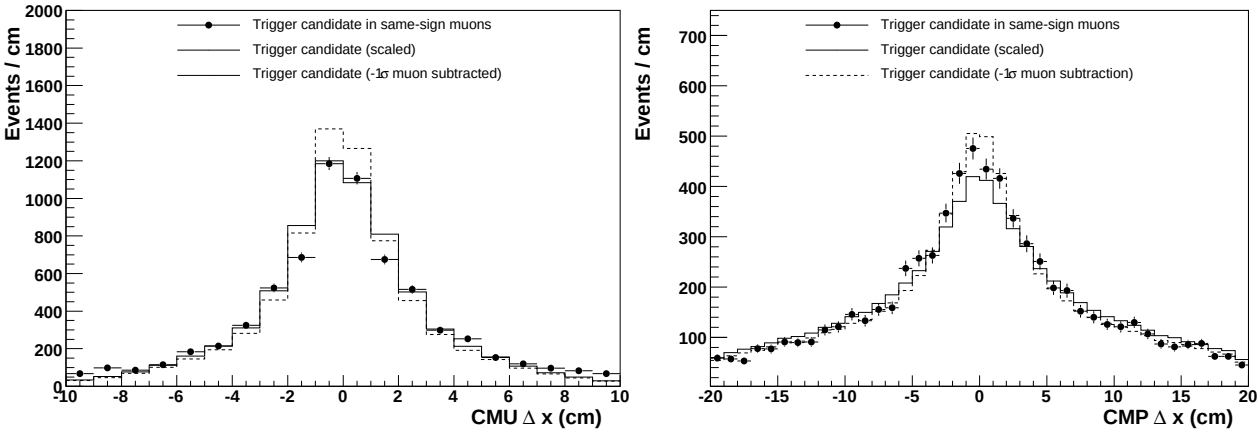

Figure 14: The CMU (left) and CMP (right) Δx distributions for the same-charge sample (circles) and inclusive trigger sample (solid histogram). The distributions are shown after removing the expected muon contamination. Also shown is the inclusive trigger sample with -1σ of the expected muons removed (dashed histogram).

π or K p_T	DIF (pre-COT)	DIF (post-COT)	Sail-through	Punch-through	Total
3 GeV	0.01%	0.12%	0.01%	0.09%	0.23%
20 GeV	-	0.14%	0.02%	0.33%	0.49%

Table 8: The first-principles estimates of relative rates of pions and kaons passing the muon identification requirements, for decays in flight and sail- and punch-through.

GeV muons yields a fraction about an order of magnitude lower (due to the larger γ factor).

A decay in flight in the meter between the COT and the hadronic calorimeter results in a muon with about 80% of the momentum of the measured π or K track. The resulting ≈ 2.4 GeV muon will have a high inefficiency due to range-out or multiple-scattering. Assuming 10% efficiency gives a 0.12% rate for a 3 GeV track to result in an identified muon. The identification efficiency for a 10 GeV muon is about 80%, but the probability for a decay in flight is reduced by 3/20. Thus, 0.14% of 20 GeV tracks result in decays in flight to reconstructed muons between the COT and the hadronic calorimeter.

To calculate the probability for punch-through or sail-through, we assume the probability to have no nuclear interactions in λ interaction lengths is $e^{-\lambda}$. There are 5 interaction lengths before the CMU, and an additional 3.5 interaction lengths before the CMP (due to 60 cm of steel). The sail-through probability is 0.02%; we assume the reconstruction efficiency reduces that to 0.01% for a 3 GeV track.

A particle punches through if at least one of its shower particles is reconstructed as a stub

in the muon chambers. The shower depth has an energy dependence, and we assume that on average a 3 (20) GeV particle punches through if it showers in the last 2 (4) interaction lengths. Applying a 60% reconstruction efficiency gives a 0.09% probability for punch-through of 3 GeV particles. The reasonably tight Δx cuts suppress punch-through of 20 GeV particles. The hadronic shower size is of the order of the interaction length, or about 20 cm in steel, while the CMP Δx cut is 5 cm. Assuming 30% of the 20 GeV particles punch through and pass the Δx cuts, the fraction of 20 GeV tracks reconstructed as a muon is 0.33%.

From Table 8, we find that decays in flight after the COT and punch-through are the primary sources of reconstructed muons originating from pions and kaons. The rate for 3 GeV tracks can be compared to the measured low-p_T fake rate, after accounting for the roughly 60% fiduciality of the CMUP detector (Sec. 3.3) included in the measurement. After this correction, the measurement of $(0.098 \pm 0.035)\%$ is consistent with the first-principles estimate of $0.6 \times 0.23\% = 0.14\%$. We can also compare the 20 GeV fake ratio to the first-principles estimate by first calculating the total background before the Δx cuts. Dividing all sources except punch-through by the Δx efficiency of 90%, and the punch-through sources by 30%, gives an estimated fake ratio of 0.50, consistent with the measurement of 0.52 ± 0.12. While these estimated values could vary significantly by adjusting the various assumptions, we find that a sensible choice of unknown parameters gives values consistent with the measurements.

3.3 Drell-Yan Production

We model Drell-Yan production using the PYTHIA Z/γ^*+ jet processes, setting the minimum process p_T to 13 GeV. Based on communication with Steve Mrenna, we use version 6.325 to allow a minimum generated mass of 210 MeV, and require the Z/γ^* to decay to muon pairs. The standard Willis tune for the boson p_T and the Rick Field tune for the underlying event are included in the generation. We apply a HEPG filter of $p_T > 17$ GeV and $|\eta| < 1.2$ for one of the generated muons. Out of 100 million generated events, 11.5 million pass the filter.

The Drell-Yan background is normalized using the Z boson peak in the data (Fig. 15). The Z boson data are selected by requiring one trigger muon and a second minimum ionizing muon candidate with $p_T > 20$ GeV that is fiducial to the COT and not to the CMUP. The non-fiduciality requirement unambiguously defines the trigger muon, and no trigger efficiency correction is therefore required. The non-fiducial candidate in the normalization sample must have EM energy < 2 GeV, hadronic energy < 6 GeV, ≥ 3 axial and stereo COT superlayers with ≥ 5 hits, and opposite charge to the trigger muon. We require $81 < m_{\mu\mu} < 101$ GeV and a minimum dimuon p_T of 40 GeV to be in the perturbative regime of the QCD radiation. As a systematic test of the normalization, we vary the dimuon p_T to 20 GeV or 60 GeV. We find a 10% variation in the overall normalization with this procedure. For an additional cross-check, we compare generator-level dimuon mass and p_T distributions with those from Sherpa $Z/\gamma^*+ \geq 1$ jet events, and find good agreement.

A scale factor correction based on Fig. 3 is applied to the second muon in the low-

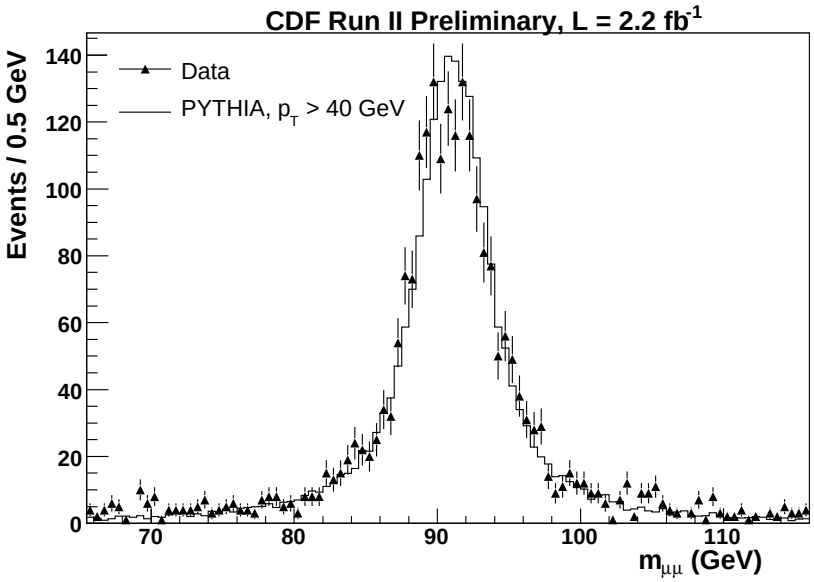

Figure 15: The mass distribution of opposite-sign muon candidates with $p_T^{\mu\mu} > 40$ GeV. The PYTHIA sample is the same Drell-Yan sample used to model the high-p_T low-mass region. We do not apply any resolution or scale corrections to the muon p_T, which has slightly better resolution in MC than in the data.

mass search sample to account for the stub and track-stub matching Δx requirements. We investigate the loose muon identification using events with a trigger muon and a track in the J/ψ mass region. The track must have $p_T > 3$ GeV and $|\cot\theta| < 0.7$. Applying the loose muon requirements to this track and taking the ratio of events gives us the product of the muon chamber fiducial acceptance and the loose identification efficiency. By fitting the J/ψ mass region to a gaussian plus a first-degree polynomial (Fig. 16), we find the acceptance times efficiency to be 60.6% (62.4%) in data (MC). The simulation thus models loose muons to better than 3% accuracy, which is negligible compared to other uncertainties.

4 PYTHIA and EvtGen Heavy-Flavor Validation

Previous studies [13, 14] have used the HERWIG generator and QQ decay package to model heavy-flavor sources of leptons at low mass. We investigate the consistency of the PYTHIA-EvtGen combination with HERWIG-QQ and with published measurements. A few small corrections are derived to match results of CDF measurements of B and D hadron production.

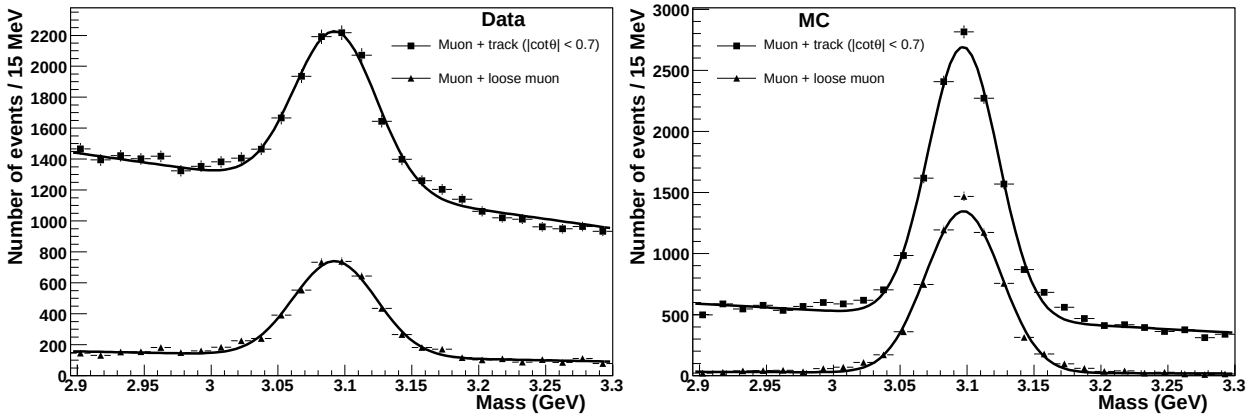

Figure 16: The mass distributions of data (left) and MC (right) events with a trigger muon and a second track (squares) or a loose muon (triangles), in the vicinity of the J/ψ mass region. The distributions are fit with a first-degree polynomial and a gaussian.

4.1 PYTHIA Heavy-Flavor Production

Tables 3 and 7 show the sources of PYTHIA muon production at the hadron level. To compare with the study in [13], we determine the sources of dimuons, single high-p_T muons, and $B^{\pm}$ hadrons at the matrix-element level. These sources can be categorized as follows: direct $b\bar{b}$ or $c\bar{c}$ production; flavor excitation, where a b or c quark results from the evolution of light-flavor quarks or gluons to the Q^2 of the hard scatter; and light-flavor (LF), where b or c quarks can result from a split gluon emitted in a light-flavor hard scatter.

Table 9 shows the relative fraction of matrix-element processes producing muons and $B^{\pm}$ hadrons in PYTHIA. The sample of $B^{\pm}$ hadrons is obtained with a HEPG filter requiring a $B^{\pm}$ with $p_T > 15$ GeV after PYTHIA dijet generation. Comparison of the muon $p_T > 2.5$ GeV and $p_T > 17$ GeV rows shows that the increased p_T requirement enhances b-quark production relative to c-quark production. Requiring a second muon further suppresses charm production and enhances $b\bar{b}$ production and gluon splitting.

A previous study from Run I [13] fit the parton-level processes obtained from HERWIG to data selected with a $p_T > 8$ GeV muon within an $E_T > 15$ GeV jet, and a second $E_T > 15$ GeV jet in the event. The default HERWIG results are shown in Table 10 and those after the fit are given in Table 11. We have insufficient statistics in our low-p_T muon PYTHIA sample to make the same event requirements as the Run I study, but we can make similar requirements of a $p_T > 8$ GeV muon and an $E_T > 10$ GeV jet. The results with and without the jet requirement are included in Table 11 for comparison.

Table 11 suggests that $b\bar{b}$ production and b excitation are reasonably well modelled in PYTHIA, but that gluon splitting is underrepresented and replaced by charm production. We expect the effect of such mismodelling of the mix of processes to be alleviated by the background normalization using $B^{\pm} \to J/\psi K^{\pm}$ decays, which will recover some of the b-

Parton	Dir. $b\bar{b}$	b Exc.	LF	Dir. $c\bar{c}$	c Exc.
μ ($p_T > 17$ GeV)	15.0%	42.6%	28.6%	2.9%	11.0%
$\mu\mu$ ($p_T^{\mu 1(\mu 2)} > 20$ (3) GeV)	21.6%	36.7%	37.8%	1.6%	2.2%
$B^{\pm}$ ($p_T > 15$ GeV)	21.0%	54.0%	24.5%	0.0%	0.4%
$B^{\pm} \to \mu X$ ($p_T^{\mu} > 17$ GeV)	21.7%	52.9%	24.9%	0.0%	0.4%
$B^{\pm} \to \mu X \to \mu\mu X$ ($p_T^{\mu 1(\mu 2)} > 20$ (3) GeV)	34.3%	43.4%	21.9%	0.0%	0.3%
μ ($p_T > 2.5$ GeV)	15.0%	25.6%	29.0%	7.5%	22.3%
$B^{\pm} \to \mu X$ ($p_T^{\mu} > 2.5$ GeV)	29.2%	49.0%	21.5%	0.1%	0.3%

Table 9: The relative sources of $B^{\pm}$ hadrons and (di)muons in PYTHIA QCD processes generated with p_T thresholds of 15 GeV (top 5 rows) and 1 GeV (bottom 2 rows). HEPG filters of μ $p_T > 17$ GeV, $B^{\pm}$ $p_T > 15$ GeV, and μ $p_T > 2.5$ GeV were respectively applied to the top 2, middle 3, and last 2 rows.

Parton	Dir. $b\bar{b}$	b Exc.	LF	Dir. $c\bar{c}$	c Exc.
μ ($p_T > 8$ GeV)	17.7%	34.9%	30.3%	4.1%	13.0%
$\mu\mu$ ($p_T^{\mu 1(\mu 2)} > 8$ (2) GeV)	17.5%	40.6%	40.0%	0.0%	1.9%

Table 10: The relative sources of single muons (Table III in [13]) and muon pairs (Table II in [14]) in HERWIG QCD processes generated with a p_T threshold of 13 GeV.

Parton	Dir. $b\bar{b}$	b Exc.	$g \to b\bar{b}$	Dir. $c\bar{c}$	c Exc.	$g \to c\bar{c}$
Run I data fit	15.5%	31.3%	24.5%	3.6%	12.5%	12.6%
PYTHIA (jet $E_T > 10$ GeV)	15.4%	35.2%	11.6%	7.3%	19.7%	9.6%
PYTHIA (inclusive)	18.7%	43.6%	14.6%	3.8%	12.1%	5.9%

Table 11: The relative sources of single muons in a HERWIG fit to Run I data events with a $p_T > 8$ GeV muon within an $E_T > 15$ GeV jet. For comparison, PYTHIA results are shown with and without a jet requirement.

quark production. To obtain a concrete estimate of the impact of underrepresenting gluon splitting, we reweight the PYTHIA events to match the relative fractions obtained in the Run I data fit. We find that the background in the opposite-charge sample increases by 1930 events, within our uncertainty of 2649 events (Table 14).

Differences in production mechanisms could manifest themselves in a mismodelling of the B-hadron p_T distribution, potentially affecting our background prediction. We compare

Sample	p_T Range	PYTHIA Events	Weighted Events	CDF cross section
D^0	$5.5 - 20$ GeV	13970	16065 ± 1492	25.6 ± 1.5 μb
$D^\pm$	$6 - 20$ GeV	3558	5154 ± 502	8.2 ± 0.4 μb
J/ψ	$2 - 6.5$ GeV	501	880	1.4 ± 0.1 μb

Table 12: The numbers of events in PYTHIA samples of 79 million generated events filtered on D^0 or J/ψ mesons. The J/ψ events are weighted to correct for the deficiency in the EvtGen $B \to J/\psi X$ branching ratio (Sec. 4.2) and to match the CDF measurement of the relative production of prompt J/ψ mesons to those from B-hadron decays. The D^0 ($D^\pm$) events are weighted by 1.15 (1.45), such that the weighted ratio of PYTHIA events is consistent with the ratio of cross sections from CDF measurements [8, 15].

the PYTHIA prediction of this distribution to the CDF differential cross section measurement $d\sigma/dp_T$ using the $J/\psi K$ decay channel [12]. In the relevant p_T range (above 15 GeV), the measurement is divided into two bins, below and above 25 GeV. The CDF measurement of the cross section ratio $\sigma(p_T^B < 25 \text{ GeV})/\sigma(p_T^B > 25 \text{ GeV})$ is 7.1 ± 1.2, and the PYTHIA prediction is 5.6. While the measurement is consistent with the prediction, we reweight the $B^\pm$ and B^0 p_T to match the measurement. The reweighting reduces the background prediction by 13%, which we take as a systematic uncertainty.

The normalization of the low-p_T PYTHIA sample uses J/ψ decays. By matching the measured prompt fraction of J/ψ production to the CDF measurement [8], we fix the relative fraction of muons from B decays. The other dominant source of muons in the low-p_T sample comes from D decays (Table 7). We investigate the normalization of D production by generating three samples of 79 million events each, separately applying D^0, $D^\pm$ and J/ψ filters to each. Table 12 shows the relative cross sections produced by PYTHIA and the corresponding CDF measurements [8, 15]. We apply a weight of 1.15 (1.45) to D^0 ($D^\pm$) events to match the ratio of CDF measurements of D^0 ($D^\pm$) [15] to J/ψ production [8].

4.2 EvtGen Heavy-Flavor Decay

The background prediction relies on the B hadron decay model in EvtGen, in particular the kinematics and branching fraction of the normalization mode $B^\pm \to J/\psi K^\pm$ and the semileptonic modes $B \to \mu X$. Since the muon subtraction in the low-p_T fake rate calculation is normalized using J/ψ decays, the $B \to J/\psi X$ branching ratio is also important.

We calculate the branching fractions of generated $B^\pm$ and B^0 hadrons using dedicated HEPG filters for these particles after PYTHIA dijet generation. The results are compared to the values obtained by the Particle Data Group [16] and shown in Table 13. All branching ratios are consistent with the PDG values except for $B \to J/\psi X$, which is 40% low in EvtGen. The EvtGen deficit arises because only a small fraction of the exclusive $B \to J/\psi X$ decays have been directly measured, so the remaining fraction must be tuned using

Decay	EvtGen BR	PDG BR
$B^{\pm} \to J/\psi K^{\pm}$	0.1018%	$0.1007 \pm 0.0035\%$
$B^{\pm} \to \mu X$	10.91%	$10.99 \pm 0.28\%$
$B^{0} \to \mu X$	10.04%	$10.33 \pm 0.28\%$
$B \to J/\psi X$	0.777%	$1.094 \pm 0.032\%$

Table 13: The branching ratios of relevant B hadron decay modes in EvtGen and the PDG.

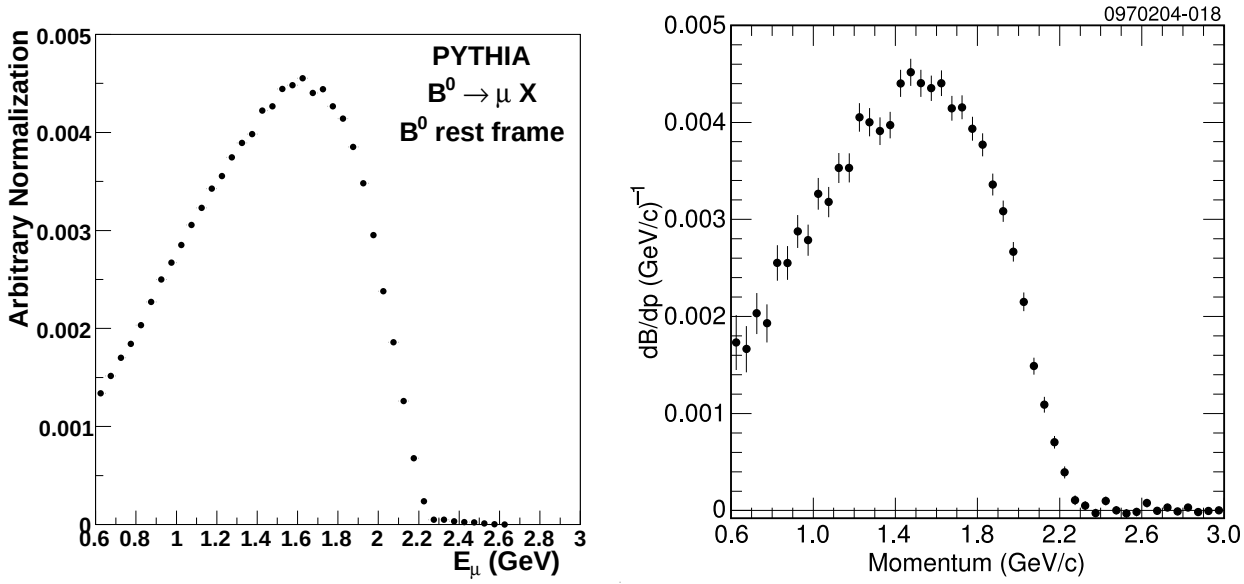

Figure 17: Left: The muon energy distribution in the rest frame of the B^0 meson in semileptonic decays modelled with EvtGen. Right: The measured electron momentum in the semileptonic decays of B^0 mesons produced from the decay of $\Upsilon(4S)$ resonance [17].

quark-level decays. The tuning in our version of EvtGen does not have sufficient b-quark decay to charm to produce a J/ψ fraction consistent with the PDG. To correct for this deficit, we weight $B \to J/\psi X$ events (except $B^{\pm} \to J/\psi K^{\pm}$) by a factor of 1.4 in the generated samples.

We investigate the EvtGen decay kinematics using the pythia sample filtered on B^0 mesons with $p_T > 15$ GeV (Sec. 4.1). Focusing on the semileptonic B decay, we boost the decay muon to the B rest frame and compare the muon's energy with the CLEO measurement of the electron momentum in the semileptonic decay of B hadrons produced from decays of the $\Upsilon(4S)$ resonance [17]. Figure 17 shows good agreement between the distributions.

The decay of directly produced J/ψ mesons is relevant for the pythia-based muon subtraction of the minimum bias sample, since we use $J/\psi \to \mu\mu$ events for normalization. We

test the modelling of this decay in the PYTHIA sample with the low-p_T muon filter ($p_T^\mu > 2.5$ GeV) by comparing the $\cos\theta^*$ distribution to a published CDF measurement [18]. The measurement determines the parameter α, defined as:

$$dN/d\cos\theta^* \propto 1 + \alpha\cos^2\theta^*, \tag{7}$$

where θ^* is the angle of μ^+ in the J/ψ rest frame with respect to the J/ψ momentum vector in the lab frame. The measurement finds $\alpha = -0.004 \pm 0.030$ (-0.015 ± 0.030) for J/ψ p_T between 5 and 6 (6 and 7) GeV. Given the relatively low statistics of the PYTHIA minimum bias sample, we combine these bins and obtain a value of $\alpha = -0.12 \pm 0.13$ for J/ψ p_T between 5 and 7 GeV in the PYTHIA sample. This value is consistent with the CDF measurement. We expect the J/ψ to be unpolarized (i.e., $\alpha = 0$) below 5 GeV as well; in the PYTHIA sample $\alpha = 0.01 \pm 0.06$ for J/ψ p_T between 3 and 5 GeV.

5 Results

We compare the total estimated background to the high-p_T low-mass dimuon data separately for same-charge and opposite-charge muons. The total numbers of events in these two samples are shown in Tables 14 and 15, with consistency between data and the background prediction. The mass distribution of the data is well described by the prediction in both samples, as shown in Figs. 18 to 21.

CDF Run II Preliminary, L = 2.2 fb^{-1}

Source	Events
Heavy-flavor hadron decays	9240 ± 2649
Trigger π or K	2826 ± 659
Drell-Yan	3758 ± 384
Low-p_T π or K	1700 ± 745
Total Background	17524 ± 2856
Data	17783

Table 14: The number of data events and the total expected background in the opposite-charge high-p_T low-mass dimuon sample.

6 Future Studies

There are a number of additional studies that can be performed to improve the sensitivity of the search to both general and specific models. Generally, the inclusion of the CMX trigger and the factor of two more available data promise the most significant gains. Specifically, we

CDF Run II Preliminary, L = 2.2 fb^{-1}	
Source	Events
Trigger π or K	1634 ± 380
Low-p_T π or K	1066 ± 474
Heavy-flavor hadron decays	144 ± 43
Total Background	2844 ± 609
Data	3128

Table 15: The number of data events and the total expected background in the same-charge high-p_T low-mass dimuon sample.

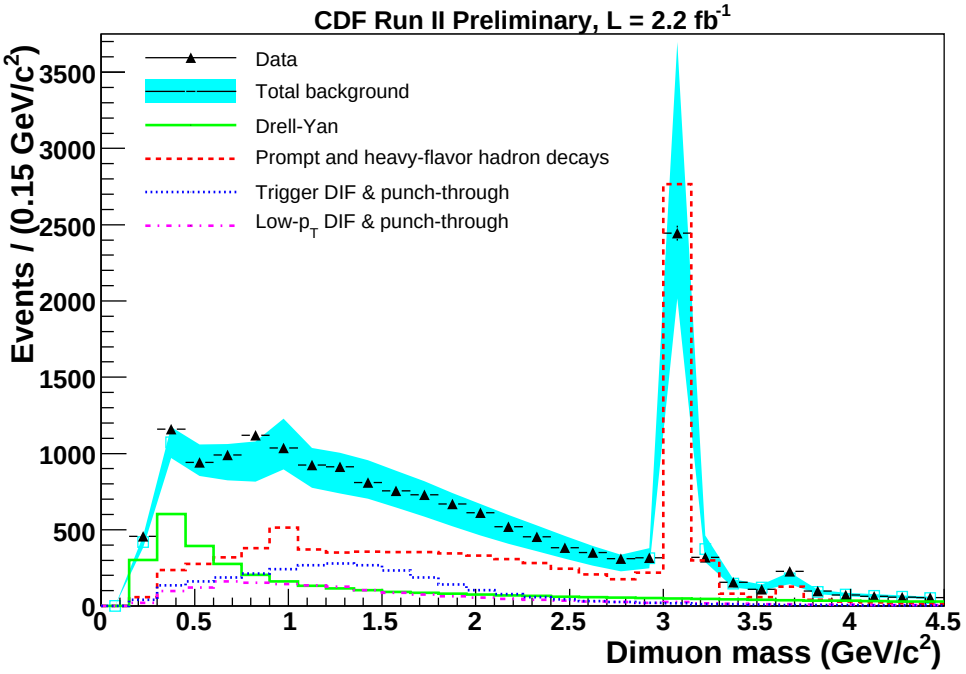

Figure 18: The mass of two opposite-charge muon candidates in a cone for data and expected background for $m_{\mu\mu} < 4.5$ GeV. The individual backgrounds have typical relative uncertainties of 25% (heavy-flavor and π/K) and 10% (Drell-Yan) in a given bin.

can optimize for the production of a Higgs decaying to pseudoscalars, $H \to aa \to \mu\mu X$ or to new low-mass gauge bosons coupling weakly to standard-model particles. When Monte Carlo for the latter becomes available, it will provide a useful test model for demonstrating the sensitivity of the search and comparing to other experiments. The model makes specific

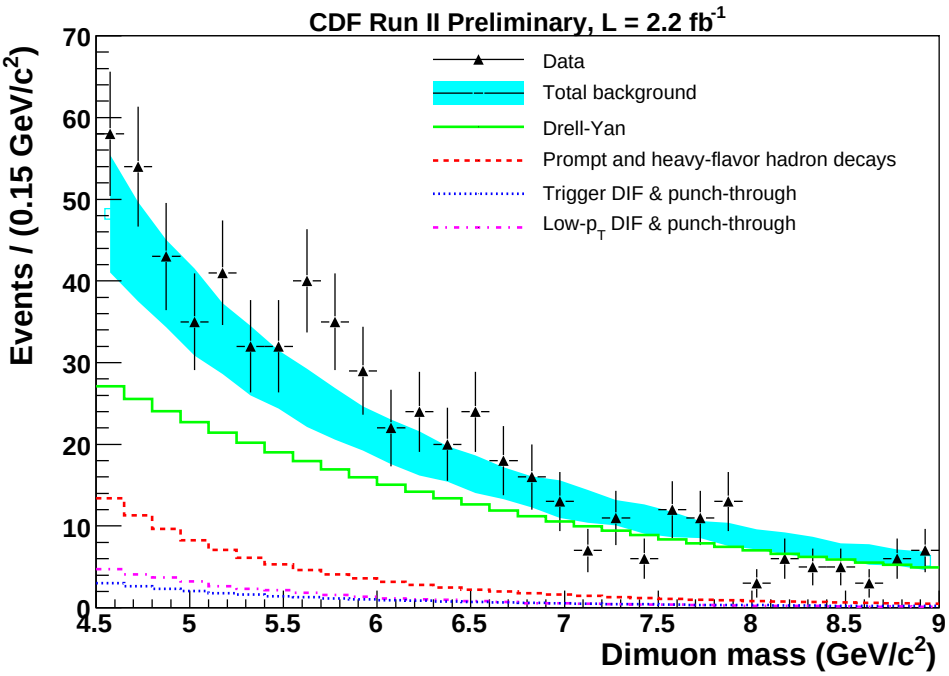

Figure 19: The mass of two opposite-charge muon candidates in a cone for data and expected background for $4.5 \leq m_{\mu\mu} < 9$ GeV. The individual backgrounds have typical relative uncertainties of 40% (heavy-flavor), 50% (π/K), and 15% (Drell-Yan) in a given bin.

predictions about higher multiplicities of muons in a cone, so extending the search to these multiplicities will improve sensitivity to this model.

7 Acknowledgments

We thank Sinead Farrington for generating the Sherpa Drell-Yan validation sample, and Paolo Giromini for suggesting numerous studies to validate PYTHIA heavy-flavor production. We also thank Steve Mrenna for providing the PYTHIA version and parameters for generating low-mass Drell-Yan, and Jay Wacker for help in understanding the kinematics of our selection near the dimuon mass threshold.

References

[1] T. Aaltonen *et al.* (CDF Collaboration), *arXiv:0810.5357v2* (2008).

[2] G. Weidenspointner *et al.*, Astron. Astrophys. **450**, 1013 (2006).

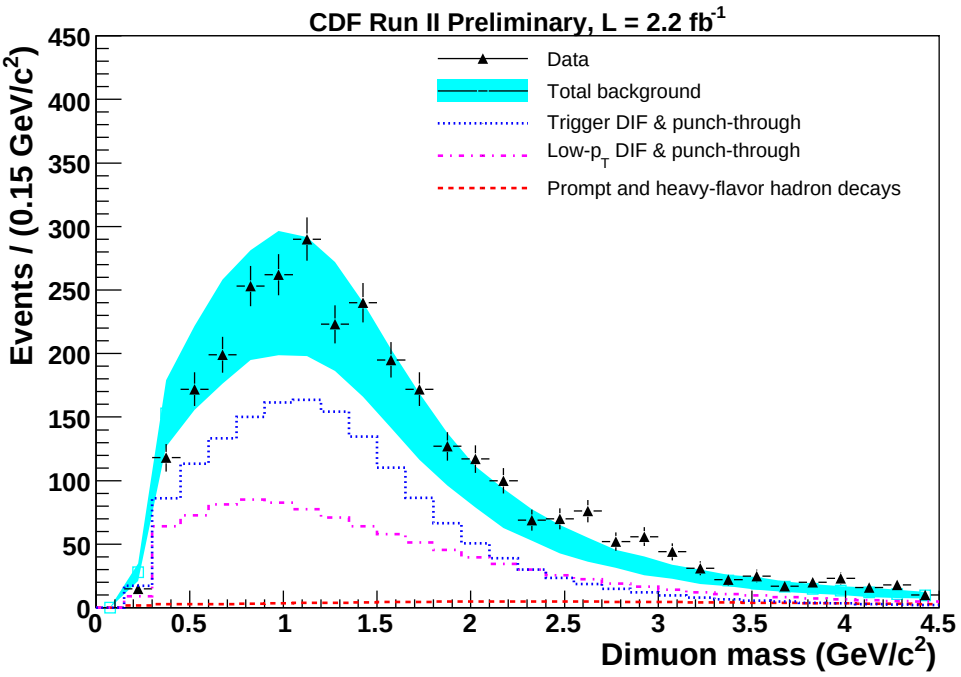

Figure 20: The mass of two same-charge muon candidates in a cone for data and expected background for $m_{\mu\mu} < 4.5$ GeV. The individual backgrounds have typical relative uncertainties of 60% (heavy-flavor) and 30% (π/K) in a given bin.

[3] O. Adriani *et al.*, Nature **458**, 607 (2009).

[4] D. P. Finkbeiner and N. Weiner, Phys. Rev. D **76**, 083519 (2007).

[5] N. Arkani-Hamed, D. P. Finkbeiner, T. R. Slatyer, and N. Weiner, Phys. Rev. D **79**, 015014 (2009).

[6] A. V. Kotwal, H. K. Gerberich, and C. Hays, Nucl. Instrum. Meth. A **506**, 110 (2003).

[7] C. Hays, A. Kotwal, Y. Li, and O. Stelzer-Chilton, CDF Note 9289 (2008).

[8] D. Acosta *et al.* (CDF Collaboration), Phys. Rev. D **71**, 032001 (2005).

[9] C. Chen *et al.*, CDF Note 6394 (2003).

[10] U. Grundler, A. Taffard, and X. Zhang, CDF Note 8262 (2006).

[11] C. Marino, K. Pitts, H. K. Gerberich, A. Taffard, CDF Note 8734 (2007).

[12] A. Abulencia *et al.* (CDF Collaboration), Phys. Rev. D **75**, 012010 (2007).

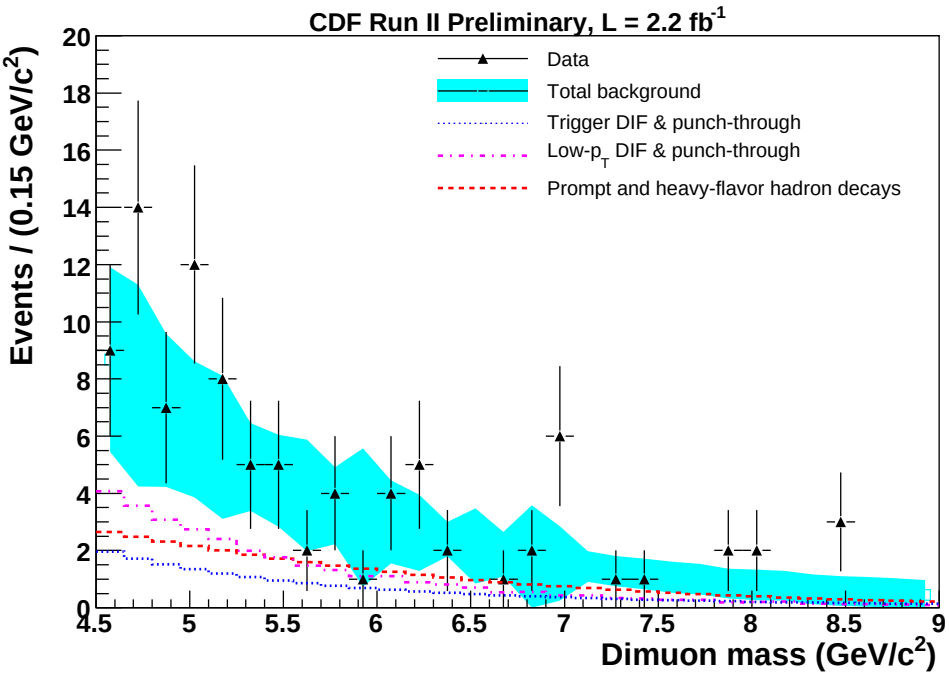

Figure 21: The mass of two same-charge muon candidates in a cone for data and expected background for $4.5 \leq m_{\mu\mu} < 9$ GeV. The individual backgrounds have typical relative uncertainties of 60% (heavy-flavor) and 50% (decays in flight) in a given bin.

[13] D. Acosta *et al.* (CDF Collaboration), Phys. Rev. D **69**, 072004 (2004).

[14] G. Apollinari *et al.*, Phys. Rev. D **72**, 072002 (2005).

[15] D. Acosta *et al.* (CDF Collaboration), Phys. Rev. Lett. **91**, 241804 (2003).

[16] C. Amsler *et al.* (Particle Data Group), Phys. Lett. B **667**, 1 (2008).

[17] A. H. Mahmood *et al.* (CLEO Collaboration), Phys. Rev. D **70**, 032003 (2004).

[18] A. Abulencia *et al.* (CDF Collaboration), Phys. Rev. Lett. **99**, 132001 (2007).